Euronoise 2018
Crete

Characterization of acoustic scattering from objects via near-field measurements

Antoine Richard[(a)], Efren Fernandez-Grande, Jonas Brunskog, Cheol-Ho Jeong
Acoustic Technology, Department of Electrical Engineering, Technical University of Denmark, Kongens Lyngby, Denmark.

Summary
Acoustic scattering is defined as the disturbance of a given incident sound field due to an object's shape and surface properties. The effect of scattering can be expressed in terms of a scattered sound field, which is calculated as the difference between the sound field when the object is present and the incident field without the object. The scattered sound field obeys Sommerfeld's radiation condition. Therefore its radial dependence (spherical decay) and its angular dependence can be separated in the far-field. The angular component, so-called the far-field pattern, is a complex directivity function, which is uniquely determined by the scattering object for a given incident sound field. Therefore, this quantity constitutes a good scattering measure, which includes both scattering from the surface (roughness scattering) as well as from the shape of the object (volume scattering). There are two main challenges associated to measuring the far-field pattern directly: i) it requires large distances between the object and the measurement points, and ii) the incident and the scattered fields need to be separated. In this study, we propose a method to estimate the far-field pattern via near-field pressure and particle velocity measurements. The sound field is measured on a closed arbitrary surface enclosing the object. The far-field pattern is estimated from an asymptotical formulation of the Helmholtz Integral Equation. It is possible to use either the total sound field or just the scattered part in the integral. Boundary element simulations show that the far-field patterns of different objects are correctly recovered, provided that the measurement points are less than half a wavelength apart.

PACS no. 43.20.Fn, 43.55.Br

1. Introduction

The widespread use of diffusers in room acoustics has led to the development of methods to characterize surface scattering, both for design and modeling purposes [1]. Surface scattering refers to the scattering of sound waves when they are reflected by a rough surface. The common approach to characterize it is to study the properties of the sound field reflected by the surface. The reflected sound field is most completely described by its directional distribution, as suggested for instance in [2]. However, such a distribution contains a large amount of data, which has led to the definition and the standardization of single-number coefficients (scattering coefficient [3] and diffusion coefficient [4]) in ISO [5].

The existing methods to evaluate surface scattering present three issues. The first issue is that the size of the sample is usually disregarded, which poses a problem of definition. For a finite-sized sample at low frequencies, the so-called reflected field is in fact the result of both surface scattering and edge diffraction. Measurement methods based on sample rotation, like the ISO scattering coefficient method [5], addressed this issue by preferring circular samples, so that only surface scattering varies with rotation. Mommertz also proposed an alternative scattering coefficient that compares the sample to a flat reference sample of the same dimensions [7]. However, it has been shown that this coefficient does not necessarily match other definitions of the scattering coefficient [8]. A second issue is that the sound field must generally be measured in the far-field, as the reflected field contains interference effects close to the surface [4]. The required large measurement distances can be difficult to achieve in practice. This explains the frequent use of scale models in the literature. Alternatively, Kleiner et al. made use of near-field acoustical holography to estimate the pressure in the far-field, by measuring the pressure on a plane [9]. Still, the sample needed to be mounted on a totally absorbing baffle, so that the measurement domain could be limited to a finite re-

(a) apar@elektro.dtu.dk

gion. Müller-Trapet [10] also proposed to use a spherical harmonic decomposition on the measured pressure field to extrapolate the far-field pressure, which requires a spherical configuration of microphones. The third issue is the need to separate the incident field and the reflected field. Different methods to achieve this are reviewed in [10], including time windowing, subtraction and sound field separation, but inaccuracies can occur, especially at lower frequencies.

Scattering is a central concept in many scientific areas, including not only acoustics but also electromagnetics, optics or quantum mechanics. In general, the studied effect is volume scattering, namely the disturbance caused by the introduction of an object in a given wave field. The scattered field is defined as the difference between the total field in the presence of the object and the undisturbed field without the object. In the far-field, the scattered field can be described by a directivity function, which is uniquely defined by the object [11]. This function appears frequently in the scattering literature under different names, such as far-field pattern [11], directivity factor [12] or scattering amplitude [13]. This approach to scattering, which is common to many fields, benefits from a solid mathematical background.

This study proposes to characterize scattering due to finite-sized samples by estimating their far-field pattern under plane wave incidence. It is shown that the far-field pattern can be estimated from near-field measurements of pressure and particle velocity, with no need to subtract the incident field. Finally, for samples with a rough surface, the relation between the far-field pattern and surface scattering is examined.

The paper first reviews concepts of surface scattering and volume scattering in Sec. 2. The near-field measurement method is then presented in Sec. 3. Section 4 exposes numerical results and studies scattering by different samples. Finally, Sec. 5 discusses the relevance of the far-field pattern and its limitations.

2. Background of acoustic scattering

2.1. Characterization of surface scattering

The concept of surface scattering is extensively used in geometrical acoustics. It arises from a high-frequency model, where an incident sound wave impinges on a rough surface. The properties of the surface are inferred from the reflected field, which is commonly decomposed into a specular and a diffuse component. Two coefficients were developed to evaluate surface scattering, known as scattering coefficient and diffusion coefficient. The reflected field depends on the incident sound field, so these coefficients are defined for specific incidence conditions, typically a free-field oblique incidence or a diffuse field. Many measurement methods (e.g. [4] or [7]) rely on the knowledge of a discretized angular distribution of the reflected pressure in the far-field $p(\theta_i)$, at n different positions.

The scattering coefficient s is defined as the ratio of reflected energy directed away from the specular component [3]. It is mostly used in numerical room acoustic models. The scattering coefficient depends on the definition of the specular component, which is not clear for samples of finite size. In order to isolate the specular part, several methods rely on the assumption that the specular and the diffuse component are statistically uncorrelated. That is the case of the ISO method [5] and its free-field version [3], where the diffuse component of the reflection is averaged out by rotating the sample. Alternatively, the correlation scattering coefficient introduced by Mommertz [7] is based on the correlation between $p(\theta_i)$ and the pressure distribution $p_{ref}(\theta_i)$ obtained for a reference flat sample with the same dimensions,

$$s_M = 1 - \frac{|\sum_i p(\theta_i) p^*_{ref}(\theta_i)|^2}{\sum_i |p(\theta_i)|^2 \sum_i |p_{ref}(\theta_i)|^2}. \tag{1}$$

As the comparison is made between two samples of the same dimensions, it is claimed that the calculated coefficient does not include the size effect.

The diffusion coefficient δ quantifies the uniformity of the reflection, and is of interest mostly for diffuser manufacturers and their customers. The standardized coefficient is based on the autocorrelation of the angular distribution as

$$\delta = \frac{\left(\sum_i |p(\theta_i)|^2|\right)^2 - \sum_i |p(\theta_i)|^4}{(n-1)\sum_i |p(\theta_i)|^4}, \tag{2}$$

assuming a uniform sampling of pressure [1].

Equations (1) and (2) show that both diffusion and scattering can be evaluated from the far-field pressure distribution $p(\theta_i)$. However, $p(\theta_i)$ is dependent on the size of the sample, whereas the surface scattering framework was developed for infinite surfaces. Moreover, the measurement of $p(\theta_i)$ must be performed in the far-field, so it requires large distances between the sample and the microphones.

2.2. Volume scattering theory

The problem of wave scattering by an object of finite size appears in various fields, which share a similar mathematical background. In this paper, we refer to [11] which studies inverse scattering problems in acoustics and electromagnetics.

Let a point be defined by its spherical coordinates $\mathbf{r} = (r, \Omega)$, where r is the distance to the origin and Ω is an angular direction. We consider an undisturbed sound field $p_0(\mathbf{r})$ in a medium characterized by its speed of sound c and its density ρ. The introduction of an object of finite size in the field leads to a new sound field $p_1(\mathbf{r})$, called total field. The scattered field $p_S(\mathbf{r})$ is then defined as

$$p_S(\mathbf{r}) = p_1(\mathbf{r}) - p_0(\mathbf{r}). \tag{3}$$

Note that while p_0 and p_1 exist physically, p_S is a mathematical construction.

The scattered field fulfills Sommerfeld's radiation condition, which makes it possible to express it in the far-field as

$$p_S(\mathbf{r}) \underset{r\to+\infty}{=} \frac{e^{-\mathrm{j}kr}}{r}\left(f_\infty(\Omega) + O\left(\frac{1}{r}\right)\right). \quad (4)$$

Equation (4) shows that the radial and the angular dependence of p_S can be separated in the far-field. The radial part decays as a spherical wave, whereas the angular part $f_\infty(\Omega)$ is a complex directivity function, called far-field pattern in [11]. For a given undisturbed sound field p_0, the far-field pattern is uniquely determined by the object, and is therefore directly linked to the scattering properties of the object. As f_∞ is a complex function, it contains more information than the common energy directivity functions in the literature, such as in [2].

3. Methodology

We aim at following the object scattering approach presented in Sec. 2.2 to estimate the far-field pattern of acoustic samples. The far-field pattern is estimated from near-field measurements of pressure and particle velocity, using the Helmholtz integral equation. We focus on flat samples, whose upper surfaces have diffusing or absorbing properties. The measurement includes both the effects of the sample's geometry and the surface properties.

3.1. Helmholtz integral equation and application

Let S be a surface enclosing the scattering object. The Helmholtz integral equation relates the scattered pressure at a given position $\mathbf{r}$ to the sound field on S. Outside of the surface, the scattered pressure is [11]

$$p_S(\mathbf{r}) = \iint_S \left(p_S(\mathbf{r_S})\frac{\partial G(\mathbf{r},\mathbf{r_S})}{\partial n} - \frac{\partial p_S(\mathbf{r_S})}{\partial n}G(\mathbf{r},\mathbf{r_S})\right) ds(\mathbf{r_S}), \quad (5)$$

where $\frac{\partial}{\partial n}$ is the normal derivative with respect to the surface S, and G is a Green's function, solution to the Helmholtz equation, which is assumed known analytically. If no source is enclosed by S, then Eq. (5) is also valid when p_S is replaced by the total field p_1 in the integral.

In Eq. (5), $\mathbf{r}$ only appears in $G(\mathbf{r},\mathbf{r_S})$. Furthermore, assuming G is a radiating solution, it follows the same form as Eq. (4) in the far-field,

$$G(\mathbf{r},\mathbf{r_S}) \underset{r\to+\infty}{=} \frac{e^{-\mathrm{j}kr}}{r}\left(G_\infty(\Omega,\mathbf{r_S}) + O\left(\frac{1}{r}\right)\right). \quad (6)$$

G_∞ can be understood as the far-field pattern of G for a point source at position $\mathbf{r_S}$, and it can be calculated analytically.

Consequently, the far-field pattern can be expressed from Eq. (5) by setting r to $+\infty$ and by using Eq. (6). The term $\frac{e^{-\mathrm{j}kr}}{r}$ can then be factorized, and by identification, one obtains

$$f_\infty(\Omega) = \iint_S \left(p_S(\mathbf{r_S})\frac{\partial G_\infty(\Omega,\mathbf{r_S})}{\partial n} - \frac{\partial p_S(\mathbf{r_S})}{\partial n}G_\infty(\Omega,\mathbf{r_S})\right) ds(\mathbf{r_S}). \quad (7)$$

Again, Eq. (7) is valid when p_1 is used instead of p_S in the integral, provided that there are no sources inside S. Furthermore, $\frac{\partial p}{\partial n}$ is related to the normal particle velocity u_n through Euler's equation, so Eq. (7) can also be expressed as a function of the pressure and the normal particle velocity on the surface S.

3.2. Measurement method

We make use of Eq. (7) to estimate the far-field pattern of a sample. We assume that it is possible to measure both the pressure and the normal particle velocity on a surface S enclosing the sample at M discrete positions $\mathbf{r}_j (1 \leq j \leq M)$. Equation (7) can be discretized to obtain a matrix equation in the form

$$\mathbf{f}_\infty = \mathbf{A}\mathbf{p} + \mathbf{B}\mathbf{u_n}, \quad (8)$$

where $\mathbf{p}$ and $\mathbf{u_n}$ are vectors of size M containing the measured pressures and particle velocities and $\mathbf{f}_\infty$ contains the estimated far-field pattern at discrete angular directions $\Omega_i (1 \leq i \leq N)$. The matrices $\mathbf{A}$ and $\mathbf{B}$ are calculated from Eq. (7). In this study, the integral is approximated as a Riemann sum, where S is subdivided in elements of equal size δs and each element is assigned a measurement point $\mathbf{r}_j$, so that

$$A_{i,j} = \frac{\partial G_\infty(\Omega_i,\mathbf{r}_j)}{\partial n(\mathbf{r}_j)}\delta s, \quad (9)$$

$$B_{i,j} = \mathrm{j}\rho ck G_\infty(\Omega_i,\mathbf{r}_j)\delta s, \quad (10)$$

with $1 \leq i \leq N$ and $1 \leq j \leq M$. Other finer interpolation strategies are of course possible.

So far, no assumption is made on the incident field, apart from the fact that there is no source inside S. This makes it possible to use either the total field or the scattered field in the measurement vectors $\mathbf{p}$ and $\mathbf{u_n}$.

Equation (8) is a forward problem, so the far-field pattern can be easily estimated from near-field measurements and the operation is not sensitive to noise. The proposed setup does not require large measurement distances as in [2] or [4], nor the separation between the incident and the reflected fields that is needed in [9] or [10] for instance.

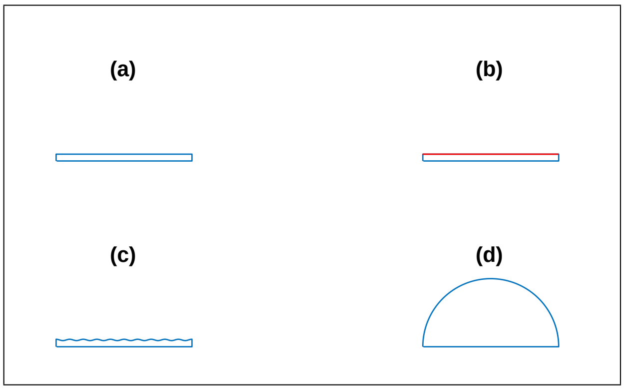

Figure 1. Tested samples. (a): flat rigid surface. (b): flat absorptive surface. (c): sinusoidal surface. (d): half-circle.

4. Numerical tests in 2D

The method presented in Sec. 3 was tested using a Boundary Element Model (BEM) in two dimensions [16]. Note that the equations were adapted, as radiating waves in the far-field follow a cylindrical decay $\frac{e^{-jkr}}{\sqrt{r}}$ in 2D. Geometries were discretized using the common rule of six elements per wavelength.

4.1. Tested samples

Samples with different scattering properties are tested, as shown in Fig. 1. For all samples, the lower boundary is a segment of length 2 m and the left and right sides are segments of length 10 cm. The samples have different upper boundaries, which are referred to as surfaces in the following, namely:

(a) flat and rigid, where the specular reflection is expected to dominate;

(b) flat and absorptive, where the surface impedance is set to ρc;

(c) sinusoidal and rigid, with an amplitude $h = 1$ cm and a period $\Lambda = 20$ cm, where we expect the energy to be redirected in specific directions;

(d) a half-circle of radius 1 m, which should redirect sound in all directions.

4.2. Simulation setup

The simulated measurement setup is shown in Fig. 2. A polar coordinate system is used $\mathbf{r} = (r, \theta)$. The samples are placed in a free-field, under normal incidence of a plane wave with an amplitude of 1 Pa. The frequency is set to 2500 Hz, corresponding to a wavelength $\lambda = 14$ cm. The choice of the measurement domain is arbitrary, but it should enclose the object. For this example, the pressure $\mathbf{p}$ and the particle velocity $\mathbf{u_n}$ in Eq. (8) are measured on a rectangle slightly larger than the sample (2.1 m×0.25 m for samples (a), (b), and (c); 2.1 m×1.25 m for sample (d)). The distance between the sampling points must be smaller than half of the wavelength to avoid aliasing effects, according to the Nyquist theorem [15]. Therefore it is set to 5 cm. Note that the discretization of Eq. (7) depends on the choice of the domain as well as the interpolation. The estimated far-field pattern $\mathbf{f}_\infty$ in Eq. (8) is sampled with a resolution of 0.5°.

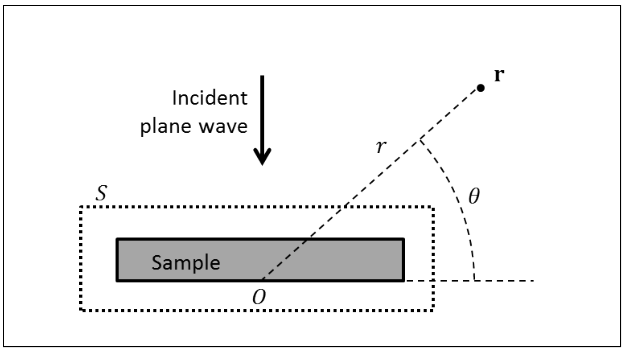

Figure 2. Simulation setup. The sample is placed in free-field. The polar coordinate system $\mathbf{r} = (r, \theta)$ is also shown.

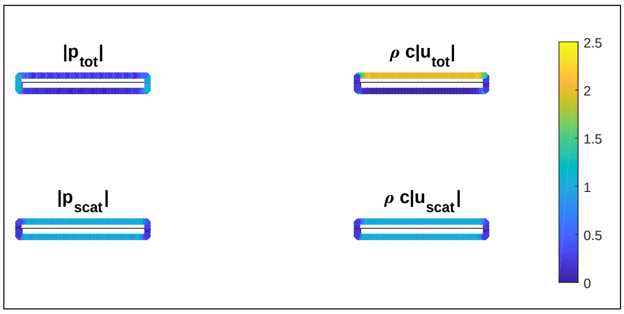

Figure 3. Amplitude in Pa of the pressure and the normalized normal particle velocity for the total field and the scattered field.

The BEM method also makes it possible to directly estimate the far-field pattern for reference: the scattered pressure is calculated on a circle of a large radius (200 m) and the radial dependence $\frac{e^{-jkr}}{\sqrt{r}}$ is compensated for.

4.3. Far-field pattern estimation

In this section, we focus on the results for test sample (a) as similar observations could be done for the other samples. Figure 3 shows the amplitude of the pressure and the normal particle velocity at the measurement points, both for the total and the scattered fields. The particle velocity has been multiplied by ρc so that it has the dimension of a pressure. For the total field, both the pressure and the particle velocity have low amplitudes below the sample, which shows that the object shadows the sound field in this region. On the upper part of the measurement domain, the total field is the result of the interference between the incident and the reflected wave, with low pressure and high particle velocity. Indeed, the distance between the upper surface of the sample and the measurement points is 10 cm, which is quite close to $\frac{3}{4}\lambda$, where the pressure would be canceled and the velocity amplitude maximal with an infinite rigid sample. With respect to Eq.

(7), the distribution of the total field indicates that, for such a large sample and at normal incidence, the far-field pattern does not depend much on the sound field below the sample. As for the scattered field, it is by definition the difference between the total field and the undisturbed field. In Fig. 3, both the scattered pressure and normal particle velocity present low amplitudes on the sides, which shows that the sample has little influence in these regions.

Figure 4 shows the estimated amplitude of the far-field pattern of the flat rigid sample as a function of θ, compared with the reference directly calculated in the BEM model. The far-field pattern is very accurately estimated from the near-field measurements, both for the scattered field and the total field as inputs, even with the rather coarse interpolation used to discretize Eq. (7). This is due to the forward nature of the problem. Results not shown here confirm that the same level of accuracy is also obtained for other shapes of the measurement domain.

4.4. Comparison of the far-field patterns

The far-field patterns of the tested samples are plotted in Fig. 5. These results are specific to the undisturbed field p_0, which corresponds to a plane wave at normal incidence in free-field. The graph can be divided into two angular domains, materialized by the vertical black dashed line.

The interval $\theta \in [0°; 180°]$ corresponds to backscattering and contains the reflection by the upper surface. It clearly shows the expected behavior of the samples, with respect to surface scattering. For the flat rigid surface, a main lobe appears in the specular direction at 90°, with side lobes due to edge diffraction. For the absorptive surface, the amplitude is very close to 0, as almost no energy is reflected back. For the sinusoidal surface, three main directions are visible. These directions agree with the theory for infinite sinusoidal surfaces [14], which states that the sound field is radiated in distinct directions θ_n. These directions fulfill the equality

$$\cos(\theta_n) = \cos(\theta_0) + n\frac{\lambda}{\Lambda}, \tag{11}$$

where θ_0 corresponds to the specular direction – 90° in this case. These directions are indicated by dotted vertical lines in Fig. 5. Finally, for the half-circle, the amplitude of the far-field pattern is quite constant, which shows that the reflected field is evenly distributed.

The interval $\theta \in [180°; 360°]$ corresponds to forward scattering and mainly shows the shadowing of the sound field by the object. Note that in the present tests, the shadowing effect is similar for all samples, due to their same overall dimensions. The half-circle result has similar main lobes to the three other samples close to 270°, but the sample's larger thickness results in marked differences on the sides.

Table I. Estimated correlation scattering coefficient s_M and diffusion coefficient δ from the backscattered part of the far-field pattern.

Samples	Flat	Absorptive	Sinsusoidal	Half-circle
s_M	0	0.999	0.294	0.978
δ	0.015	0.306	0.042	0.492

4.5. Calculation of coefficients from the far-field pattern

By definition, the far-field pattern is directly linked to the directional properties of the scattered field. More precisely, in a free-field configuration, the backscattered part of the far-field pattern ($\theta < 180°$) represents the angular distribution of the reflection by the tested surfaces. Therefore it can be used as the far-field pressure distribution that appears in Eqs. (1) and (2).

As an example, the correlation scattering coefficient and the diffusion coefficient defined in Sec. 2 were calculated for the studied samples in Table I. For the correlation scattering coefficient, the reference sample is the flat rigid one, which explains why that sample yields a value of 0. The scattering coefficient of the absorptive sample is almost equal to 1, due to the significant difference between its far-field pattern and the reference's. Note that as there is almost no reflection, the definition of the scattering coefficient as a ratio of the reflected power does not really apply here. The sinusoidal surface leads to a coefficient of about 0.3, due to the redirection of energy in a few specific directions. The half-circle yields a correlation scattering coefficient of almost 1, as expected by the amount of energy radiated in all directions and the considerably lower amplitude in the specular direction.

As for the diffusion coefficient, the lowest value is obtained for the flat rigid sample, for which the reflected energy is concentrated around the specular direction. The diffusion coefficient of the sinusoidal surface is still rather low, as the reflected field is not uniform. Both the absorptive sample and the half-circle show a higher value as their angular response is flatter.

These examples show that the far-field pattern constitutes valid information for estimating known coefficients from the surface scattering literature, if it is restricted to backscattering only. For the present examples, it was not possible to follow sample rotations methods, as they require measurements in 3D.

4.6. Angle dependence

This section investigates the influence of the angle of incidence on the far-field pattern for the sinusoidal sample (b). The far-field pattern is plotted for incidence angles 0°, 30°and 60° in Fig. 6. As in Sec. 4.4, the graphs can be divided into a backscattering part

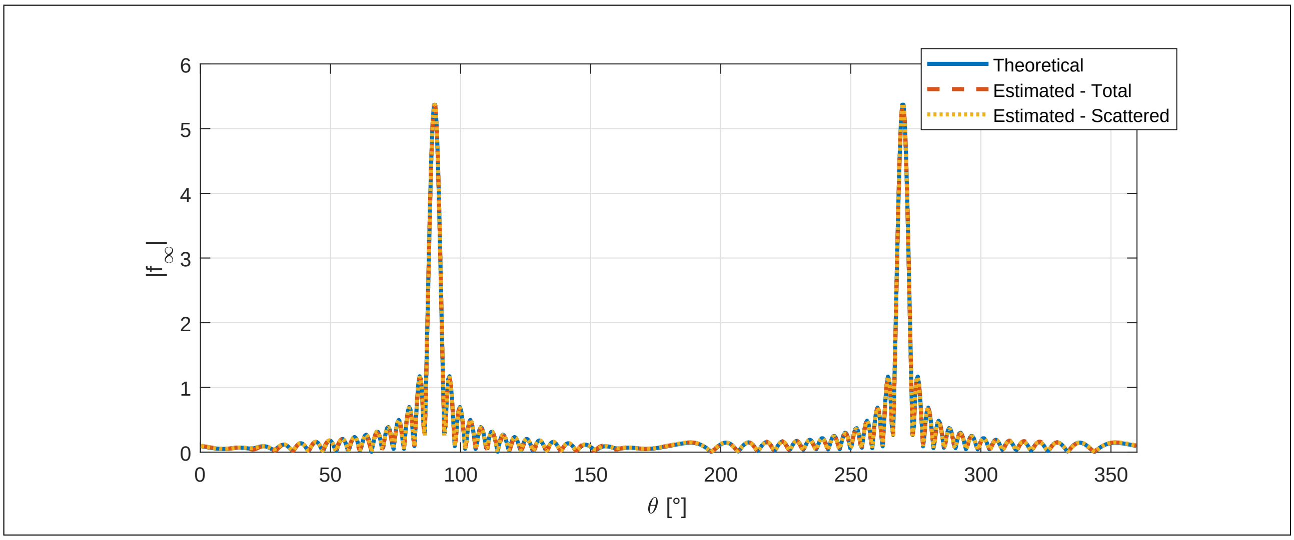

Figure 4. Estimated amplitude of the far-field pattern for the flat rigid sample. The estimation is done from the scattered field and the total field and compared with a reference calculated at 200 m.

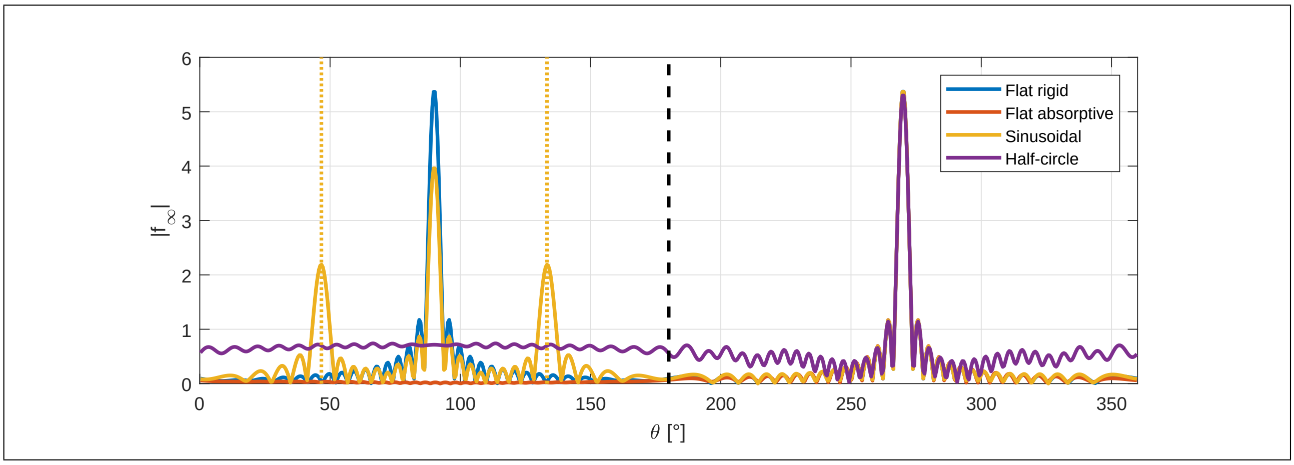

Figure 5. Comparison of the far-field pattern amplitudes of the tested samples: flat rigid, flat absorptive, sinusoidal, half-circle.

($\theta \leq 180°$) and a forward scattering part ($\theta \geq 180°$). The expected directions of the backscattered sound field from Eq. (11) are shown as dashed lines, the thickest one corresponding to the specular direction. For the three incidence angles, peaks appear at these directions. In the three graphs, the forward scattering part presents only one main peak corresponding to the direction of propagation of the incident wave.

The lobes of the far-field pattern tend to be smeared as the angle of incidence increases. This effect is partly due to the fact that at grazing incidence, the backscattered sound is also influenced by the sound field below the sample. At large angles of incidence, backscattering and forward scattering are no longer independent.

4.7. Dependence on the environment

In the previous tests, the samples were placed in a free-field. The introduction of boundary conditions in the environment modifies the undisturbed sound field p_0. As a result, the scattered field and the corresponding far-field pattern are not the same as in free-field. For instance, the sample can be placed on a rigid baffle (semi-anechoic chamber) which is common in the literature [10]. In that case, at normal incidence, the undisturbed field p_0 is a standing wave, composed of the incident plane wave and its specular reflection by the baffle. It is still possible to define a radiating scattered field and a far-field pattern.

Figure 7 shows the resulting far-field patterns for the samples studied in Sec. 4 on an infinite rigid baffle. Note that the angle θ is only defined from 0 to 180°. The effects of the different surfaces are still visible. The flat rigid sample exhibits a main lobe in the specular direction. The absorptive sample leads to a reduced amplitude of the far-field pattern. As opposed to the free-field case, it is not close to 0, because the scattered field interferes destructively with the reflection by the baffle. For the sinusoidal sample, peaks in the three expected directions are again visible . Fi-

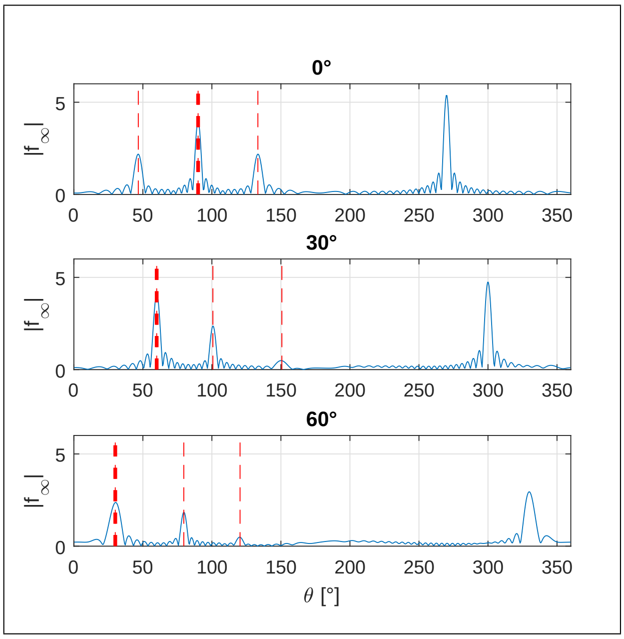

Figure 6. Far-field pattern amplitude for the sinusoidal surface and a plane wave with incidence angles 0°, 30°and 60°

nally, the half-circle shows oscillations at all angles, and the uniformity of the reflection is much less obvious than in the free-field case.

It should be noted that in this semi-anechoic setup, one cannot describe the reflected field as easily as in free-field. The reflected field is here the sum of the scattered field and the specular reflection by the baffle, which is not decaying with distance. Therefore, the far-field pattern does not represent the reflection as clearly as in the free-field case.

5. Discussion

The results of Sec. 4 show that the proposed method makes it possible to accurately estimate the far-field pattern of acoustic samples. The method does not require large measurement distances nor any processing on the measured sound field, as opposed to the existing techniques to characterize surface scattering.

The far-field pattern depends on the incident sound field, as stated in Sec. 2. That is what motivated the choice of an incident plane wave in the tests: the incident field is then defined by only one parameter, namely the direction of the plane wave. With that framework, we have information that is dependent on both incidence angle and frequency, as it is generally the case in architectural acoustics. Random incidence could then be studied by integration over the incidence angle. Nevertheless, a different far-field pattern would be obtained with a more complex incident sound field.

The far-field pattern provides a complete description of scattering by acoustic samples, including not only surface scattering, but also edge diffraction and shadowing. The fact that it includes the size effect can be of interest in architectural acoustics, as any object introduced in an environment would naturally have a certain geometry. Nevertheless, it is not possible to totally separate surface scattering from other effects in the far-field pattern. In the conditions of Sec. 4 (large samples, small incidence angles, free-field), the backscattered field constitutes a fair approximation of the reflected field by the surface, although the effect of sample size is still clearly visible as lobes in the far-field pattern.

Furthermore, it was assumed that the backscattered part did not depend on the sound field below the sample, which is not always true, for instance at large incidence angles. In the literature, the sample is commonly placed on or in a baffle (absorbing or rigid), to ensure that the back of the sample does not play any role on the scattered field. However, the baffled problem is fundamentally different from the free-field one and it cannot be used to study surface scattering directly. Further investigation is therefore needed to analyze scattering in complex environments.

6. Conclusion

This study examines the characterization of scattering by acoustic samples, using the concept of far-field pattern. This quantity is a complex directivity function that is uniquely defined by the sample and the incident field.

Numerical tests in two dimensions show that the far-field pattern can be accurately estimated from near-field measurements of both pressure and particle velocity, using either the total field or the scattered field. Samples with different surface properties were also studied in free-field under normal plane wave incidence. Numerical results show that the far-field pattern contains information on both surface scattering and edge diffraction in the backscattered directions. Surface scattering dominates due to the large size of the samples and the small incidence angle. In general, more important coupling effects occur, for example at larger angles of incidence. Finally, the same samples positioned on an infinite baffle yield different results, demonstrating the dependence of the far-field pattern on the environment.

The far-field pattern can be beneficial in architectural acoustics as it fully describes the effect of acoustic samples, including both scattering and absorption. It provides phase and directional information on the scattered sound field, which can be of interest in numerical models.

Acknowledgement

The authors would like to thank Vicente Cutanda Henríquez for providing the OpenBEM toolbox and Mélanie Nolan for comments on the manuscript.

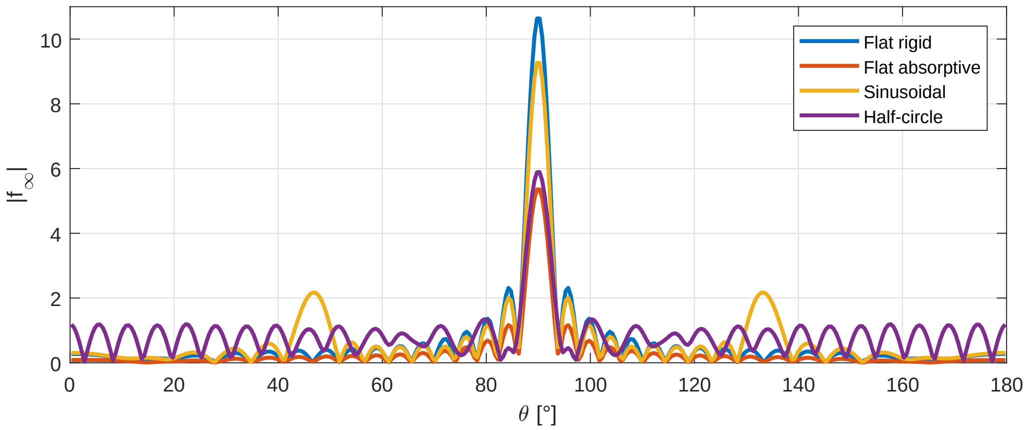

Figure 7. Comparison of the far-field pattern amplitudes of the tested samples in a semi-anechoic environment.

References

[1] T. J. Cox, B.-I. L. Dalenback, P. D'Antonio, J.-J.Embrechts, J. Y. Jeon, E. Mommertz, M. Vorländer: A tutorial on scattering and diffusion coefficients for room acoustic surfaces. Acta Acust. united Ac. 92 (2006) 1-15.

[2] P. D'Antonio, J. Konnert: The directional scattering coefficient: Experimental determination. J. Audio Eng. Soc. 40 (1992) 997-1017.

[3] M. Vorländer, E. Mommertz: Definition and measurement of random-incidence scattering coefficients. Appl. Acoust. 60 (2000) 187-199.

[4] T. J. Hargreaves, T. J. Cox, Y. W. Lam: Surface diffusion coefficients for room acoustics: free-field measures. J. Acoust. Soc. Am. 108 (2000) 1710-1720.

[5] ISO 17497: Acoustics – Sound-scattering properties of surfaces. (Parts 1 and 2).

[6] M. Vorländer, J.-J. Embrechts, L. De Geetere, G. Vermeir, M. H. de Avelar Gomes: Case studies in measurement of random incidence scattering coefficients. Acta Acust. united Ac. 90 (2004), 858-867.

[7] E. Mommertz: Determination of scattering coefficients from the reflection directivity of architectural surfaces. Appl. Acoust. 60 (2000) 201-203.

[8] T. Sakuma, Y. Kosaka: Comparison between scattering coefficients determined by specimen rotation and by directivity correlation. International Symposium on Room Acoustics: Design and Science 2004.

[9] M. Kleiner, H. Gustafsson, J. Backman: Measurement of directional scattering coefficients using near-field acoustic holography and spatial transformation of sound fields. J. Audio Eng. Soc. 45 (1997) 331-346.

[10] M. Müller-Trapet: Measurement of surface reflection properties: concepts and uncertainties. PhD Thesis, Aachen, 2015.

[11] D. Colton, R. Kress: Inverse acoustic and electromagnetic scattering theory. Springer, 2013.

[12] G. A. Kriegsmann, A. N. Norris, E. L. Reiss: An 'optical' theorem for acoustic scattering by baffled flexible surfaces. J. Sound Vib. 99 (1985), 301-307.

[13] A. Levitas, M. Lax: Scattering and absorption by an acoustic strip. J. Acoust. Soc. Am. 23 (1951), 316-322.

[14] R. L. Holford: Scattering of sound waves at a periodic, pressure-release: An exact solution. J. Acoust. Soc. Am. 70 (1981) 1116-1128.

[15] E. G. Williams: Sound radiation and nearfield acoustical holography. Academic Press, 1999.

[16] V. Cutanda Henríquez, P. M. Juhl: OpenBEM - An open source Boundary Element Method software in acoustics. Proc. Internoise 2010.